Final Draft
of the original manuscript:

Mohedano, M.; Blawert, C.; Yasakau, K.A.; Arrabal, R.; Matykina, E.;
Mingo, B.; Scharnagl, N.; Ferreira, M.G.S.; Zheludkevich, M.L.:

Characterization and corrosion behavior of binary Mg-Ga alloys

In: Materials Characterization (2017) Elsevier

DOI: 10.1016/j.matchar.2017.03.040

Characterization and corrosion behavior of binary Mg-Ga alloys

Marta Mohedano[a,c*], Carsten Blawert[a], Kiryl A. Yasakau[b], Raul Arrabal[c], Endzhe Matykina[c], Beatriz Mingo[c], Nico Scharnagl[a], Mario G.S. Ferreira[b], Mikhail L. Zheludkevich[a,b]

a. Magnesium Innovation Centre, Institute of Materials Research, Helmholtz Zentrum Geesthacht, Max-Planck-Str. 1, D-21502 Geesthacht, Germany

b. Department of Materials and Ceramic Engineering/CICECO – Aveiro Institute of Materials, University of Aveiro, 3810-193 Aveiro, Portugal

c. Departamento de Ciencia de Materiales, Facultad de Química, Universidad Complutense, 28040 Madrid, Spain

*Corresponding author. Tel: +494152871956+; Fax:+ 494152871960

E-mail: mmohedan@ucm.es

Abstract

Four binary cast Mg-Ga alloys containing 1, 2, 3 and 4 wt.% Ga were studied in terms of microstructure and degradation behavior. The alloys present two types of intermetallics: (i) the second phase Mg_5Ga_2, which volume increases with the amount of Ga in the alloy, and (ii) inclusions containing impurities. For the first time, the binary Mg-Ga system is analyzed paying particular attention to the effect of secondary phases (Mg_5Ga_2) and impurities on the localized corrosion mechanism using AFM/ SKPFM. Inclusions containing impurities reveal a high Volta potential difference, enough to form an active galvanic couple. However, localized electrochemical activities decrease with time leading to uniform degradation. For short immersion times, there is no clear influence of the element Ga on the corrosion behavior, measured by electrochemical and hydrogen evolution tests. However, for longer immersion times, increasing the amount of Ga in the alloy shows a clear negative effect. Electrochemical measurements reveal that higher Ga containing alloys form faster an oxide layer which is not stable.

Keywords

Mg alloys; Galium; Microstructure; Atomic force microscopy (AFM); Corrosion

1. Introduction

There is an increasing interest in magnesium alloys as potential candidates for structural applications (lightweight vehicles and electronic devices) and also for biomedical purposes (biodegradable implants) [1]. Traditionally, aluminum containing alloys have been considered the most representative of magnesium commercial alloys due to their good castability and reasonable corrosion and mechanical properties at room temperature [2]. In particular, the AZ91, AM50 and AZ31 have been deeply investigated [3-5]. In order to overcome some of the limitations of Mg-Al alloys, such as low creep resistance, Al toxicity in humans, and insufficient corrosion resistance under specific environments, new alloy systems are being investigated. The latter normally include additions of rare earths, Zn, Sn, Ca and Sc, among others, resulting in improved corrosion and mechanical properties [6,7].

An interesting novel alloying element is gallium, which is the next element after aluminum in the boron group in the periodic table of elements. So far, the number of studies on Mg-Ga alloys is rather limited. There is some very early work regarding the phase diagram Mg-Ga summarized by Beck [8], which was updated by Nayeb-Hashemi et al. [9] and Feng et al. [10]. McDonald was considering Mg-Ga and Mg-Ga-Mn as ductile alloys for sheet material and provided some mechanical data [11] and more recent mechanical results are given for Mg-2Ga alloy [12].

In terms of applications, most of the research is focused on the use of Mg-Ga systems as sacrificial anodes in seawater batteries [13,14]; also, there is some information about their use for hydrogen storage [15]. In the case of applications for sacrificial anodes, Ga addition promotes the electrochemical activity of Mg due to a faster dissolution of Mg anode in environments containing aggressive ions [16-18]. In particular, for Mg-Ga-Hg combinations, the activation of the α-Mg dissolution was associated with the presence of secondary phases ($Mg_{21}Ga_5Hg_3$ and Mg_5Ga_2) inducing the electrochemical activities and a dissolution-

redeposition process [19,20]. However, the corrosion mechanism remains unclear in terms of localized electrochemical activities around these phases and in particular for the binary system Mg-Ga, the role of secondary phases has not been studied.

In addition, Mg-Ga materials would also qualify for applications in medical implants [21,22]. The first study about the potential use of binary Mg-Ga, Mg-In and Mg-Sn alloys as biomaterials was recently suggested [23]. Binary alloys based on Mg-Ga showed the best results for mechanical and corrosion properties measured in 0.9 wt.% NaCl solution. Moreover, cytotoxicity tests indicated that Ga had the lowest toxicity, followed by Sn and In, pointing out the promising use of Mg-Ga based materials as biodegradable implants. In principle, gallium seems to be non-toxic and even therapeutic effects such as bone resorption and formation, modulation of immune activity and inhibition of some cellular proliferation are reported [24]. Also, Ga element has been already approved by Food and Drug Administration (FDA) to treat hypercalcemia of malignancy [25].

Due to the particular characteristics of Ga element, its addition into Mg alloys could open new possibilities for alloy design and applications. However, up to date, the corrosion mechanism of Mg-Ga system has not been studied in detail. In the present work, four Mg-Ga alloys (with 1, 2, 3 and 4 wt.% Ga additions) are evaluated in terms of characterization and corrosion behavior. For the first time the binary Mg-Ga system is analyzed paying particular attention to the effect of secondary phases and impurities on the localized corrosion mechanism.

2. Experimental procedure

2.1 Test material

All castings of the binary magnesium alloys were prepared in Helmholtz Zentrum Geesthacht (Germany) by gravity die casting from commercially available high purity Mg (HPMg) as starting material (HPMg: 0.0021 Fe, 0.0073 Si, 0.0006 Ni, 0.0042 Cu, 0.0046 Al, 0.0160 Mn, in wt.%, and Mg balance). The pure Mg was melted under Ar/SF_6 protective gas and held at 675°C before the nominal gallium contents from 1 to 4 wt.% were added (Ga: 0.0009 Bi, 0.005 Mg, 0.009 Mn, 0.21 Fe, 0.009 Si, 0.03 Ce, 0.02 Sb, 0.005 Co, in wt.%, and Ga balance). The melt was allowed to cool down to 650°C before pouring it into the steel die which was hold at 300°C. The die allows casting of finger bars with 18 mm diameter and 200 mm length.

The compositions of the castings were determined and controlled by a combination of spark spectrum emission analysis (for the heavy metal contaminations) and EDS large area analysis (for Ga). The compositions of the four alloys used in the present study are given in Table 1.

Table 1. Composition analysis in wt. % for the studied materials using spark spectrum emission analysis (for the heavy metal contaminations) and EDS large area analysis (for Ga)

	Elements wt. %							
	Ga	Al	Cu	Mn	Fe	Ni	Zn	Si
Mg-1Ga	1.3	0.0107	0.00179	0.046	0.00247	0.00065	0.0958	0.0237
Mg-2Ga	2.2	0.0142	0.00168	0.0476	0.0025	0.00055	0.0053	0.0269
Mg-3Ga	3.1	0.0131	0.00139	0.0457	0.00263	0.00024	0.0052	0.02
Mg-4Ga	3.9	0.0135	0.00133	0.047	0.00274	0.00021	0.00499	0.0198

2.2 Specimen preparation and characterization

For metallographic characterization, specimens were ground through successive grades of silicon carbide abrasive papers from P500 to P4000, followed by polishing (3 μm OPS with 1μm diamond paste). For optical analysis, a light optical microscopy Leica DMI 5000 was used

and specimens were etched with picric acid solution to reveal the constituents of the alloys. Samples were coated with an ultra-thin gold layer and examined by scanning electron microscopy (SEM) using a Tescan Vega3 SB and JEOL JSM-6400 operating at 20 kV and equipped with Energy Dispersive X-ray (EDX) microanalysis hardware.

A JEOL 2000-FX transmission electron microscope (TEM) operating at 200 kV and equipped with EDX microanalysis facilities was used for characterization of second phase particles. TEM specimens were prepared by ion milling disks with a diameter of 3 mm and 0.1 mm-thick in a Gatan PIPS system with a small incident angle until perforation.

Surface hardness was measured applying a load of 5 kg for 20 s by using an AKASHI AVK-AII Vickers hardness machine. The cited values are the average of ten measurements.

To understand the galvanic interactions of the different phases in the alloys and to monitor the change of surface morphology, during the initial stages of corrosion process, atomic force microscopy (AFM)/ Scanning Kelvin probe force microscopy (SKPFM) measurements were performed. Prior to the measurements, the Mg alloys were abraded on SiC papers down to P4000 grit and then polished by diamond paste down to 0.5 μm. The samples were cleaned on a soft sponge pad wetted by 2-propanol and wiped by a filter paper. After cleaning the samples were transferred to a desiccator in order to prevent corrosion. AFM/SKPFM analysis was carried out during the same day after polishing. Localized corrosion investigation was performed in the following way: (i) after preliminary study, the samples were immersed in 1 mM NaCl (open to air) during 20 and 40 min (ii) after immersion, the samples were rinsed with deionized water and the rest of the water from the surface was blotted by a filter paper. Before AFM analysis the samples were stored in a desiccator. A commercial AFM Digital Instruments NanoScope III system with Extender™ Electronic Module was used to study the evolution of topography of metal surface. SKPFM was performed to study the evolution of Volta potential

difference of Mg alloys surface before and after immersion in NaCl electrolyte. For SKPFM measurements AFM was operating in the interleave mode with two pass scans. The first scan acquired topography of the surface. During the second scan the tip was lifted off the surface to a distance of 100 nm, the piezoelectric actuator was switched off and an AC voltage of 5000 mV at the resonance frequency of a cantilever was applied between the tip and the sample to cause electrostatically induced oscillations of the cantilever. Using the nulling technique the Volta potential difference (VPD) between the alloy surface and a tip was measured to obtain a Volta potential map. Volta potential values are referenced versus an AFM probe. For all SKPFM measurements silicon probes covered with Pt-Cr layers were used. VPD potential of AFM probes was carefully checked before and after measurements against a standard metal surface. The deviations of the measured Volta potential were less than 0.04 V. Temperature and humidity levels were around 23±2ºC and 60±6% respectively during measurements.

To get further knowledge of the growing layer of corrosion products and its composition during exposure to an electrolyte X-ray photoelectron spectroscopy (XPS) was performed by using a Kratos DLD Ultra Spectrometer with an Al-Kα X-ray source (monochromator) as anode with power of 225W. The samples were used as received without any further surface preparation or cleaning and after the exposure to electrolyte after electrochemical impedance spectroscopy (EIS, 7 days of immersion in 0.5 wt.% NaCl at room temperature). For the survey spectra, a pass-energy (PE) of 160 eV was used while for the region scans PE was 40 eV. Charge neutralization was applied during all measurements. Depth profiling was carried out by using argon ion sputtering with energy of 3.8 keV and a current density of 125 μA/cm^2. The etching rate was determined to be 12 nm/min specific for Ta_2O_5. Data evaluation was done by using CasaXPS Software. The spectra were calibrated to binding energy of 284.5 eV for C-C of the C1s signal. For the depth profiling the region files were quantified without any further deconvolution due to incomplete compensation of charge caused by Ar ion etching.

2.3 Corrosion tests

For all the corrosion tests the samples were ground with P1200 grit emery paper and rinsed with water and ethanol prior to the testing.

Information about the electrochemical behavior was obtained by performing potentiodynamic polarization measurements in 0.5 wt.% NaCl solution, saturated with atmospheric oxygen. A typical three electrode cell (Ag/AgCl reference (with 3 M KCl), Pt counter and the specimens as working electrode) was used. The temperature was controlled at 22 ± 0.5°C while stirring the electrolyte during the experiments. After 30 minutes of recording of the open circuit potential (OCP), the polarization scan was started from –200 mV relative to the OCP at a scan rate of 0.2 mV/s. The test was terminated when a current density of 5 mA/cm^2 was exceeded to guarantee sufficient localised corrosion damage. From the cathodic branch of the polarization curve, the corrosion rate was calculated using the current density at the intersection of the Tafel slope with the vertical through the corrosion potential. The Tafel slope was fitted in the region of -150 to -50 mV relative to the corrosion potential. The anodic part was not used because non-Tafel behavior of the anodic part of the curve.

Afterwards EIS measurements were performed to see the ability of the alloys to recover from those defects. The parameters of the impedance measurements are described in the following paragraph.

Additional information about the protective film formation on the surface was obtained from EIS measurements up to 7 days of immersion using the same electrolyte and cell setup as described above for the polarisation measurements. Latter tests were performed at open circuit potential in the frequency range from 10.000 Hz to 0.1 using amplitudes of ± 10 mV rms and all measurements were done in triplicate. Due to large variations with time in the protective

ability of the films formed on the same alloy specimens a detailed analysis of the spectra using equivalent circuits was not performed. Instead, the impedance values at the lowest measured frequency were used to demonstrate the evolution of corrosion resistance of the different alloys with time. The low frequency impedance is mainly defined by the sum of resistive components from the oxide/hydroxide film and charge transfer resistance.

Gravimetric tests were performed during 15 days immersion in neutral 0.5 wt.% NaCl naturally-aerated solution using specimens with a working area of ~8 cm^2 that were weighed before and after the tests using a balance with an accuracy of 0.01 mg. The average corrosion rate for this period was calculated by weighing the tested specimens after pickling in a solution of 200 g/L for 1–2 min and also from the amount of hydrogen evolved during the test. Hydrogen evolution measurement is an accurate method to calculate corrosion extent since it does not require the elimination of corrosion products, where errors are easily committed. Since hydrogen is the main product of the cathodic reaction and the stoichiometry of the overall corrosion process of magnesium proves that each mol of evolved hydrogen corresponds to the oxidation of one mol of magnesium, it is relatively simple to calculate the corrosion rate from the total volume of hydrogen evolved during the test [26]. Error bars show standard deviations of triplicate measurements.

3. Results

3.1 Characterization

Optical images of Mg-1Ga alloy reveal equiaxed grains of α-Mg phase with an average size of 238±12 μm (Fig. 1 a). Grain size refinement is observed for higher Ga concentrations, with values of 180±4, 116±4 and 125±10μm for 2, 3 and 4 wt.% Ga, respectively (Fig 1 b-d).

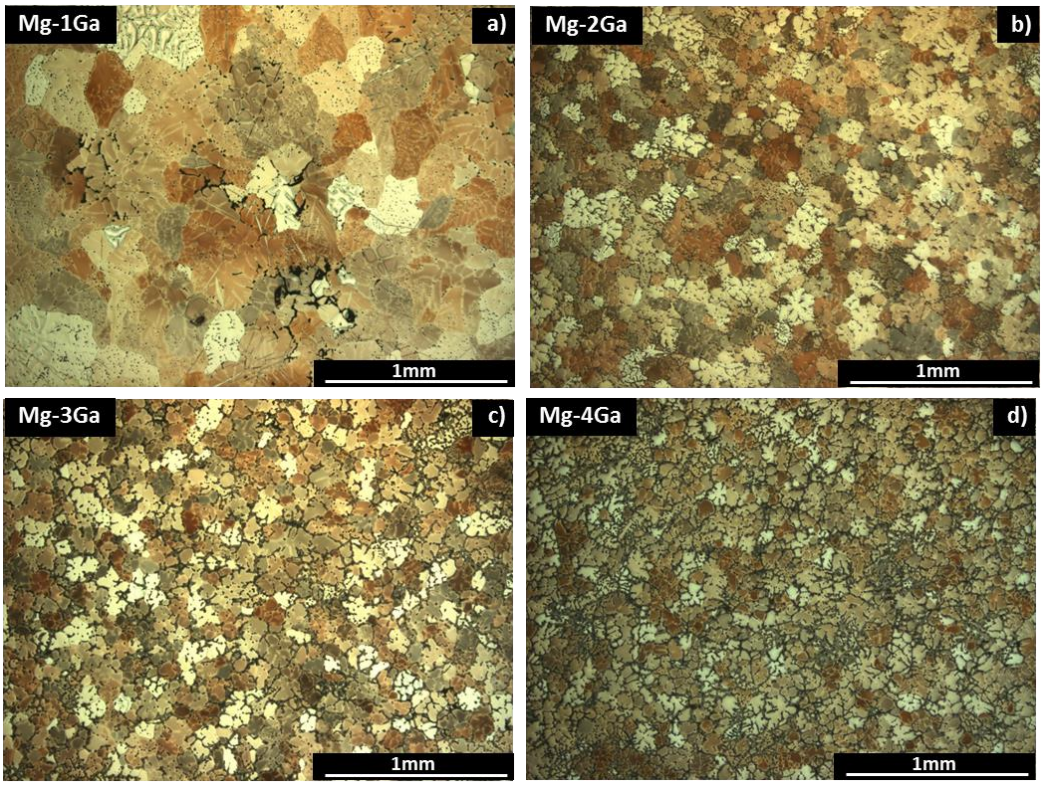

Figure 1. Optical micrographs of (a) Mg-1Ga, (b) Mg-2Ga, (c) Mg-3Ga and (d) Mg-4Ga alloys.

The area fraction of the secondary phase, identified by using TEM as Mg_5Ga_2 (Fig. 2 a,b) increases for higher Ga content. TEM study also shows the presence of polygonal-shape particles with an average size of 0.2–1 μm containing Fe and Co impurities (Fig. 2 b, c and Table 2).

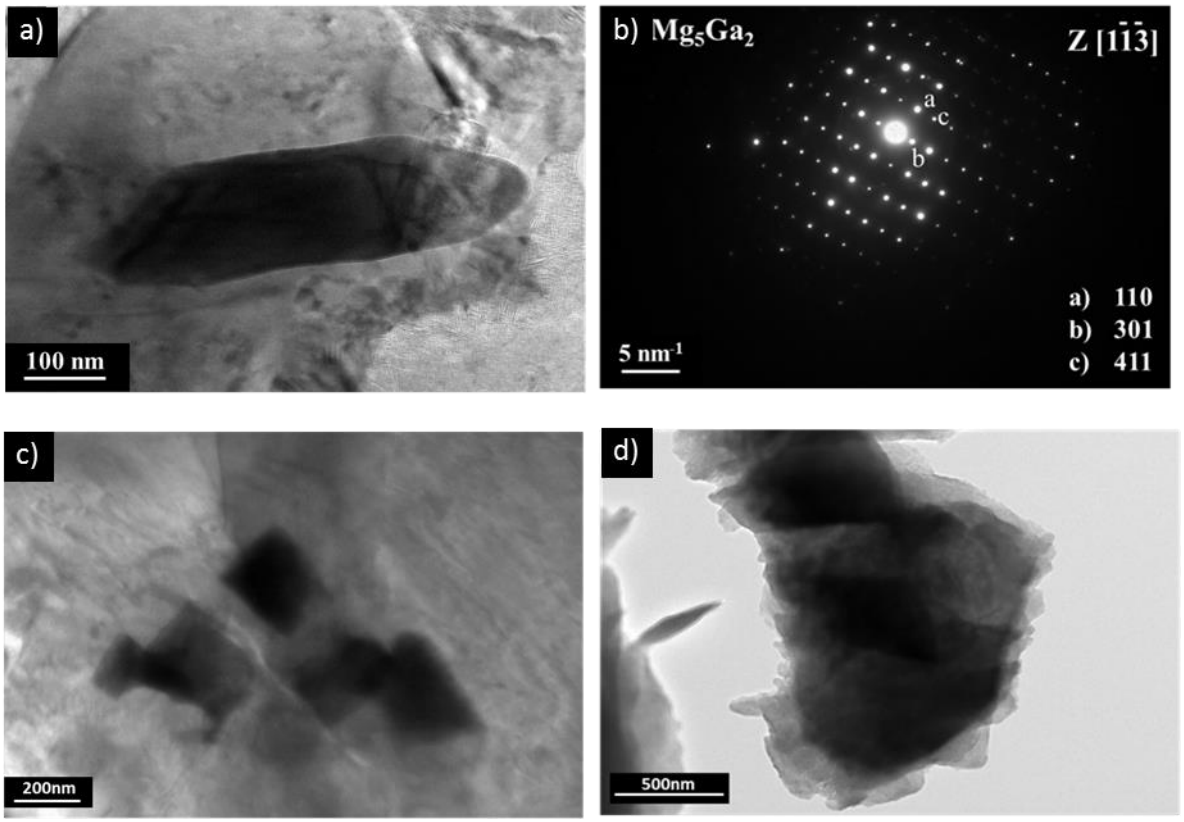

Figure 2. TEM analysis: (a) Second phase (b) electron diffraction pattern of the second phase (c,d) polygonal-shape particles containing impurities.

Table 2. Composition determined by point analysis EDS (at.%) for Figure 2 (c,d)

	Elements at. %					
	Mg	Al	Fe	Co	Ga	Zr
Image c	73.51	1.51	1.56	1.33	22	0.08
Image d	73.54	2.24	2.14	2.24	19.85	

Slightly higher hardness values are observed for the alloys with greater Ga content, mainly due to the smaller grain size of the α-Mg phase and greater amount of the Mg_5Ga_2 phase (Table 3), but the differences are not revelant.

Table 3. Hardness measurements (HV)

Material	Hardness (HV)
Mg-1Ga	49±2
Mg-2Ga	52±3
Mg-3Ga	51±3
Mg-4Ga	53±4

Figure 3 shows scanning electron micrographs of the Mg-4Ga alloy where the fine lamellar structure of the Mg_5Ga_2 second phase and Ga microsegregation in the α-Mg phase can be observed. A detail of the second phase (Fig. 3 b) with the corresponding EDS analysis (Table 4) shows that Ga concentrations varies from <7.32 at.% in the α-Mg surrounded by Mg_5Ga_2 to <1.28 at.% Ga in the centre of the grain far from the second phase.

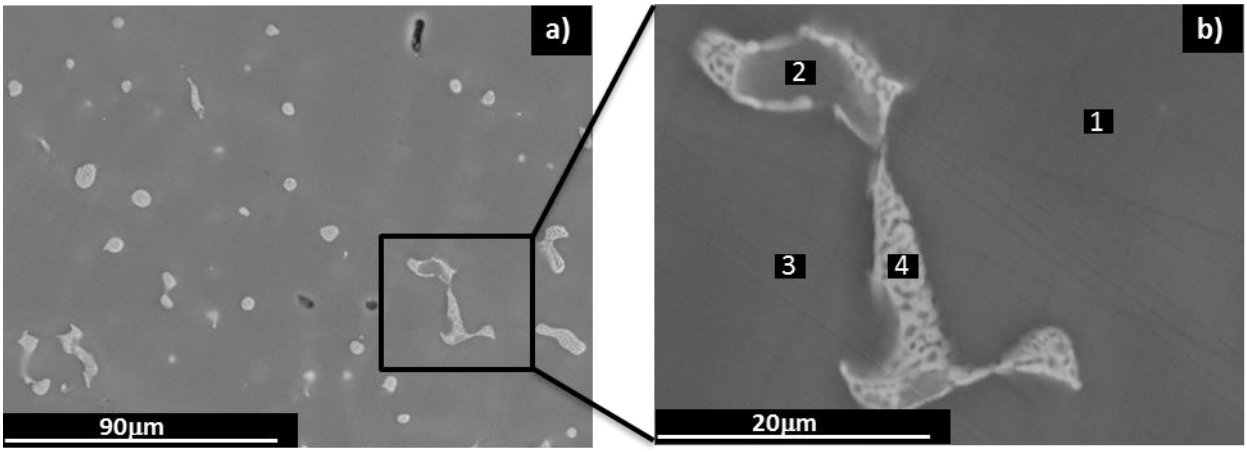

Figure 3. Scanning electron micrograph of the Mg-4Ga (a) lower magnification (b) a detail of the second phase Mg_5Ga_2.

Table 4. Composition determined by point analysis EDS (at.%) for Figure 3 b

	Elements at. %	
Point	Mg	Ga
1	98.72	1.28
2	92.68	7.32
3	98.59	1.41
4	83.88	16.12

The average Volta potential difference (VPD) for Mg-Ga alloys is about -2.02±0.04 V vs. AFM probe (Table 5). Ga addition does not significantly change the average VPD level compared with that measured on a pure Mg sample (ca -2 V). The information about the local nobility of the Mg_5Ga_2 intermetallic phase shows a cathodic behavior with a VPD around 74±15 mV vs Mg matrix level (Table 5). The variation of VPD can be related to slight changes in composition for intermetallic particles in the four alloy families.

Table 5. VPD levels on magnesium alloys, intermetallics and impurities; at least 15 different intermetallics or impurities were analysed in order to calculate ΔVPD levels.

	VPD vs. probe
Average alloy surface VPD	-2.02 ±0.04 V
ΔVPD Mg_5Ga_2 second phase	+74±15 mV
ΔVPD cathodic network	+25±5 mV
ΔVPD on large impurities	+154±34 mV

The topography image, surface potential maps and potential profiles of a large area of Mg-4Ga alloy (as an example) are shown in Figure 4. In general, shape and appearance of different intermetallic phases are similar in all 4 alloy families. Mg-4Ga alloy was selected for the discussion because it has a large amount of intermetallics which are easily found on the alloy surface. Although AFM topography maps (Fig.4 a) vaguely show the alloy microconstituents, after polishing, SKPFM map (Fig. 4 b) clearly differentiates between the bulk Mg solid solution matrix (dark region) and the Mg_5Ga_2 particles (bright regions). The intermetallic particles are preferably segregated at the grain boundaries and in Mg solid solution. Additionally, the SKPFM image also reveals impurities and areas of gallium segregation around the intermetallics. Contour lines, schematically shown on SKPFM image, emphasize the gallium segregation region. Such areas have slightly higher VPD (>20 mV) compared with the level of the bulk Mg solid solution ca. -2.02 V (Fig. 4 c and Table 5). The presence of less noble α-Mg

matrix, with a darker contrast on SKPFM image, surrounded by the the second phase (Mg_5Ga_2) (as seen in Fig. 3 b) can be also observed. Apart from Mg_5Ga_2 second phase, Mg-Ga alloys surface displays inclusions containing different impurities such as Fe, Co and others as it was observed with TEM analysis (Fig 2 c,d and Table 2).

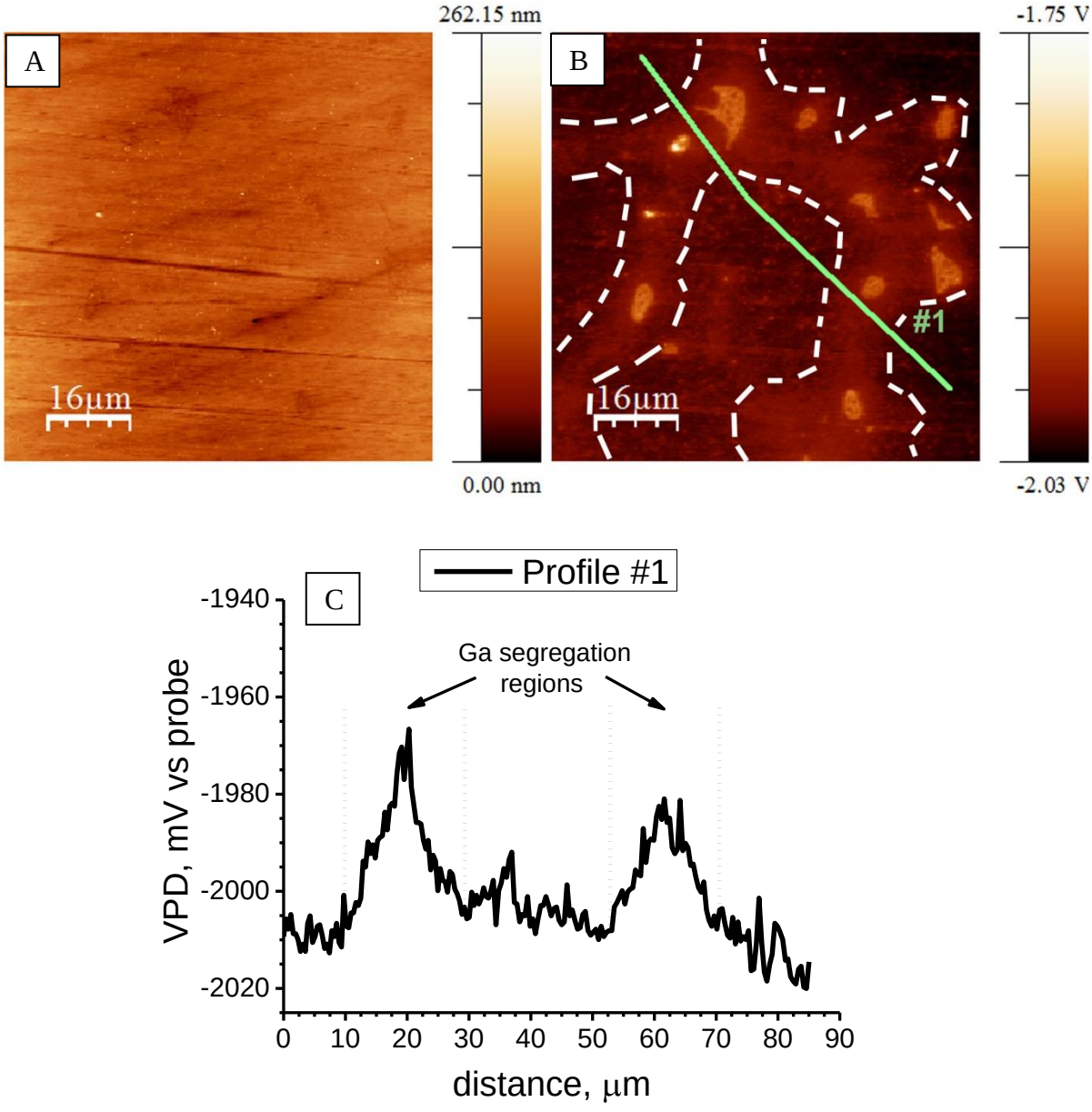

Figure 4. Mg-4Ga sample: (a) surface topography (b) SKPFM image and (c) VPD profile across the grain.

Figure 5 is an example of the second phase Mg_5Ga_2 with an inclusion containing more noble elements. Such inclusions have higher VPD levels around +154±34 mV vs. Mg matrix (Table 5). The high VPD and deviation may indicate that such phases have different composition. Figure 5 d presents EDS analysis of the inclusion and intermetallic. As can be seen the inclusion contains more noble elements such as Mn and Fe, and also some Si. In contrast, the intermetallic contains only Mg and Ga. In general, metallic phases having sufficiently high VPD vs. a metal matrix may induce a high corrosion activity of the surrounding matrix [27]. Therefore, the understanding of initial corrosion mechanisms of magnesium alloys is important for understanding the corrosion susceptibility of such alloys.

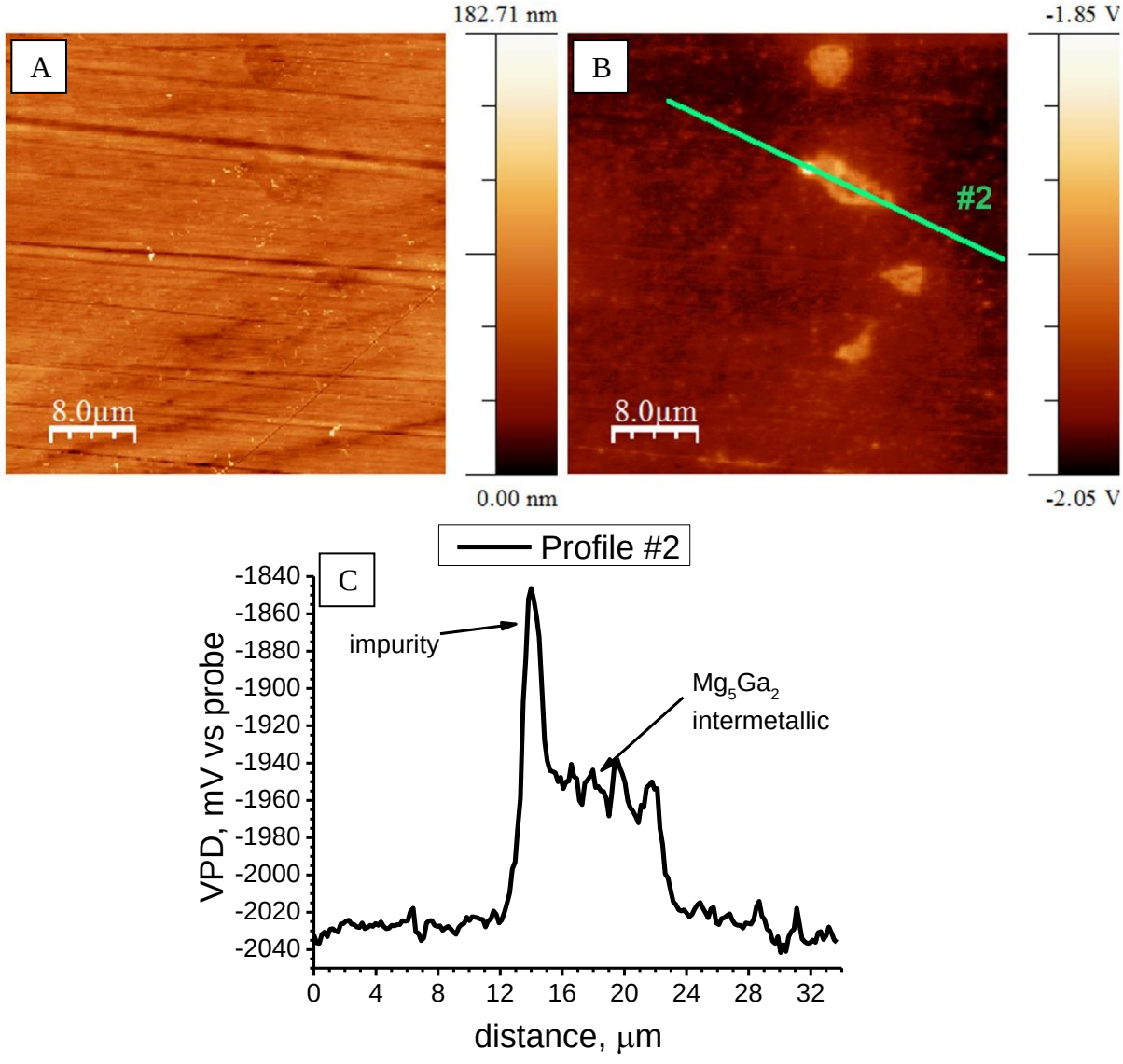

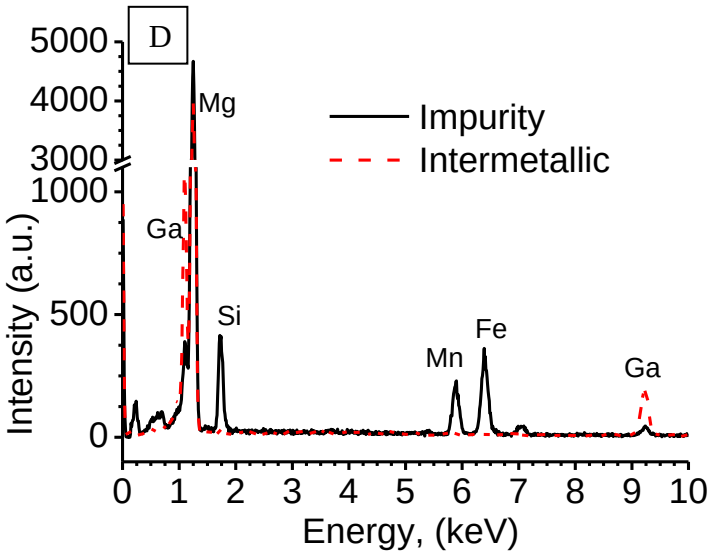

Figure 5. Mg-4Ga sample: (a) surface topography (b) SKPFM image and (c) and a VPD profile across the intermetallic and impurity; (d) EDS analysis of an impurity and intermetallic.

3.2 Corrosion results

3.2.1 AFM/ SKPFM localized corrosion measurements

The investigation of localized corrosion activity of Mg-Ga alloys was performed ex situ on microstructural level before and after immersion in diluted NaCl solution. The same metallic surface was analyzed by AFM/SKPFM before and after 20 and 40 min of immersion. The changes of the surface topography and Volta potential were observed specifically at two types of microstructural heterogeneities Mg_5Ga_2 and impurities. Since all the Mg-Ga alloys showed similar microstructural features e.g. Mg_5Ga_2 phase and impurities inclusions, the study was made on Mg-4Ga alloy only. It is worth to mention that other alloys displayed quite similar localized corrosion behavior.

Figure 6 presents the evolution of topography and VPD of Mg-4Ga alloy surface before and after immersion (20 and 40 min) in diluted NaCl solution. The initial topography does not clearly show second phase intermetallics. However VPD map shows a clear signature of

Mg_5Ga_2 second phase which has a higher VPD (brighter zones) compared to Mg matrix (Figure 6 a, d, g). After 20 and 40 min of immersion the topography maps do not show any signs of dissolution of the intermetallic particles (Figure 6 b,c). Moreover, the surface seems to be covered by a porous layer of corrosion products. XPS spectra of the samples after exposure (not shown) confirm that this layer is mainly formed by MgO and $Mg(OH)_2$. VPD maps have changed after immersion. The intermetallics have lost the VPD contrast and are no longer clearly distinguished from the surrounding Mg matrix (Figure 6 e, g). After 40 min of immersion the VPD map shows a more uniform potential distribution over Mg matrix and intermetallics (Figure 6 c, f). Such uniform VPD distribution on the surface after corrosion is most probably attributed to the screening effect provided by the surface oxide/hydroxide film.

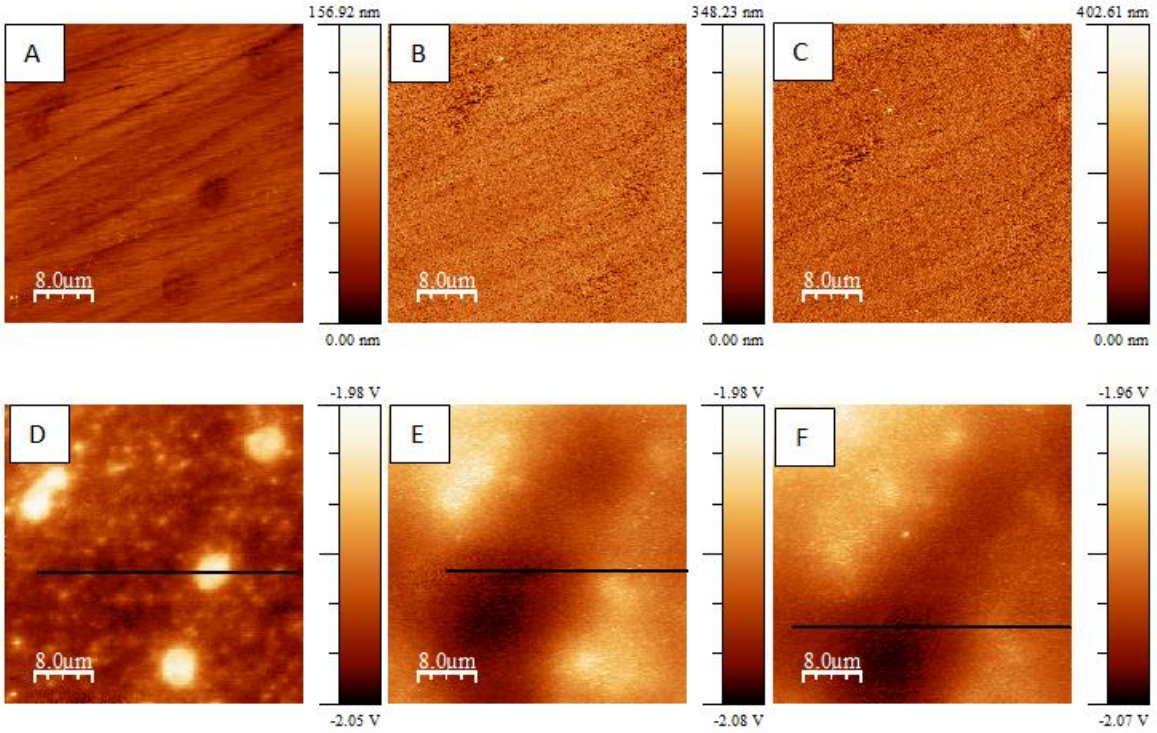

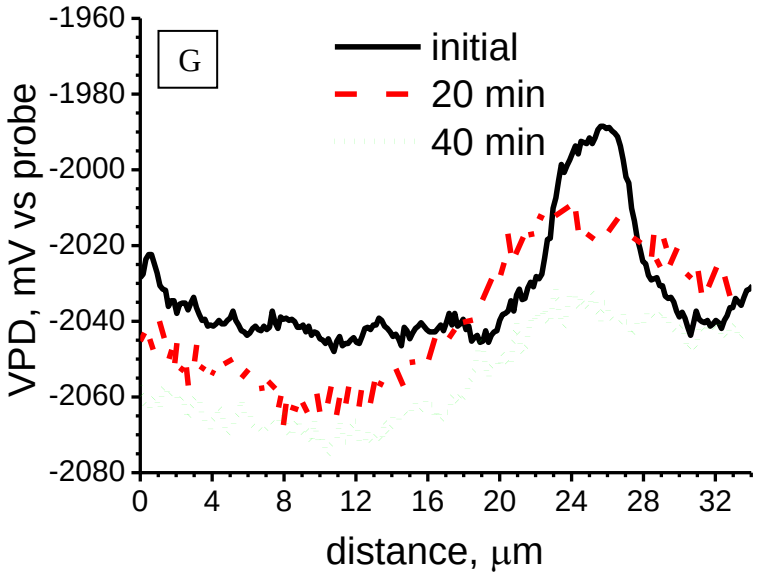

Figure 6. Mg-4Ga sample: (a,b,c) surface topography before and after immersion (20 and 40 min) in diluted NaCl solution, (d,e,f) SKPFM before and after immersion (20 and 40 min) in diluted NaCl solution (g) VPD profiles across the Mg_5Ga_2 intermetallic.

On the contrary, the localized corrosion susceptibility of inclusions containing Fe impurities reveals several important features. The impurities have higher VPD level with respect to magnesium matrix (Table 5). The more noble Volta potential of impurities reflects their cathodic behavior. Therefore, the impurities will support the reduction reactions and promote the oxidation of the Mg matrix. Indeed, the impurity has developed a cathodic activity which caused precipitation of around 2 micrometers-high $Mg(OH)_2$ corrosion product cap at the impurity after immersion (Figure 7b, c). The VPD level above the cathodic particle has significantly decreased after immersion which may be caused due to potential shielding by a tall corrosion precipitate cap (Figure 7 e, f, g).

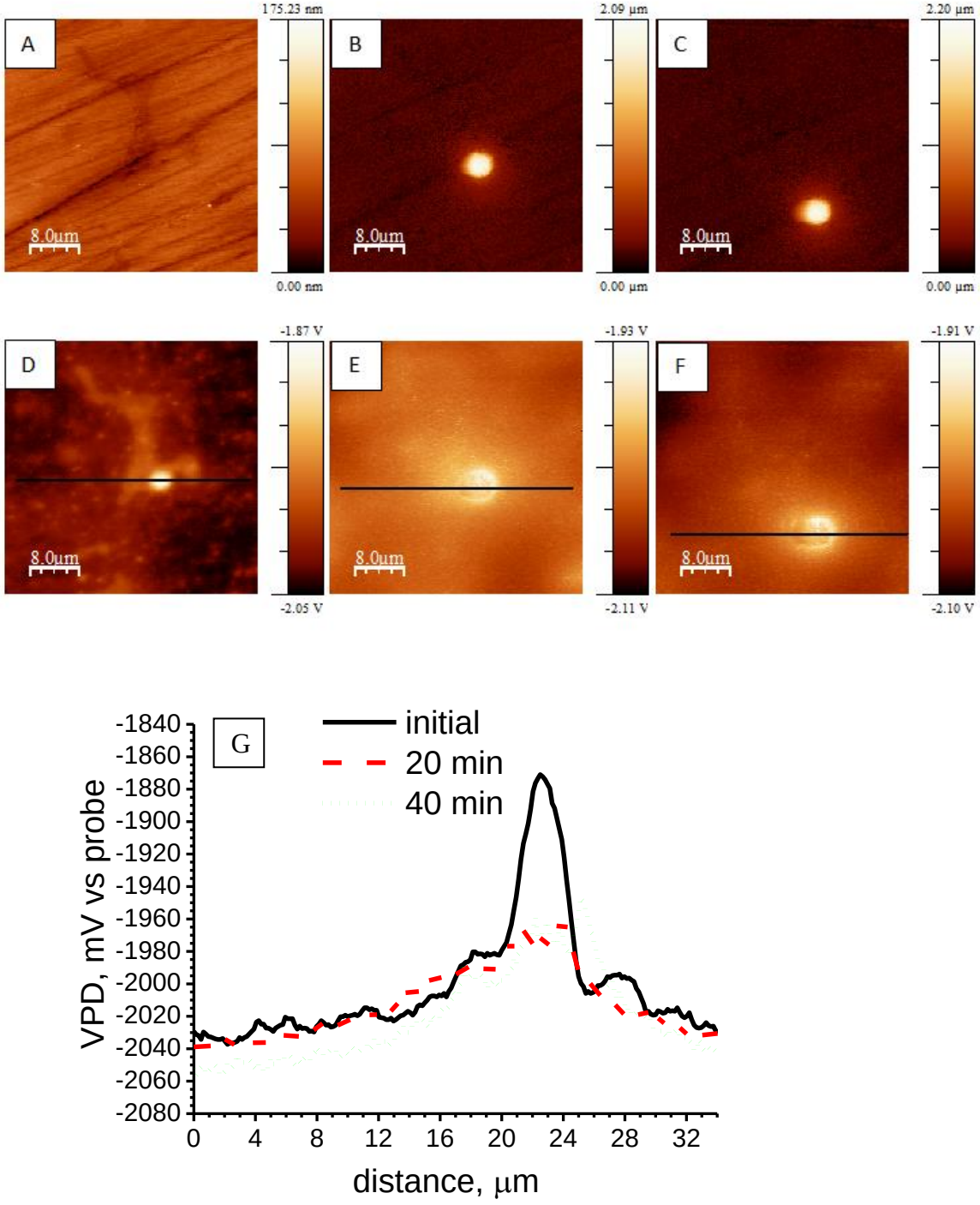

Figure 7. Mg-4Ga sample: (a,b,c) surface topography before and after immersion (20 and 40 min) in diluted NaCl solution, (d,e,f) SKPFM before and after immersion (20 and 40 min) in diluted NaCl solution (g) VPD profiles across the Mg_5Ga_2 intermetallic and impurity.

The initial corrosion attack on Mg-Ga alloys was mainly caused by the presence of cathodic impurities. In contrast, the secondary phase intermetallics did not show any remarkable local corrosion attack in spite of the higher Volta potential level than that of the Mg matrix. A study of cross-sections of samples after the immersion tests did not reveal any local attack at the interface between the secondary intermetallics and the matrix either (not shown).

3.2.2 Immersion tests: mass loss and hydrogen evolution measurements

Figure 8 shows the hydrogen volume vs time for all materials up to 15 days of immersion in 0.5 wt.% NaCl. During the early stages of immersion the studied alloys show similar hydrogen evolution rates without a clear effect of gallium concentration. However, for immersion times above 5 days, corrosion rate clearly increased with increase of the amount of gallium in the alloy. The values calculated from hydrogen evolution measurements were comparable to those obtained from mass loss results (Table 6); the slight variation is insignificant and should be considered within the experimental and method errors. Thus, the addition of 4, 3 and 2 wt.% Ga resulted in average corrosion rates after 15 days that are approx. 7, 4 and 2 times higher than that of the Mg-1Ga.

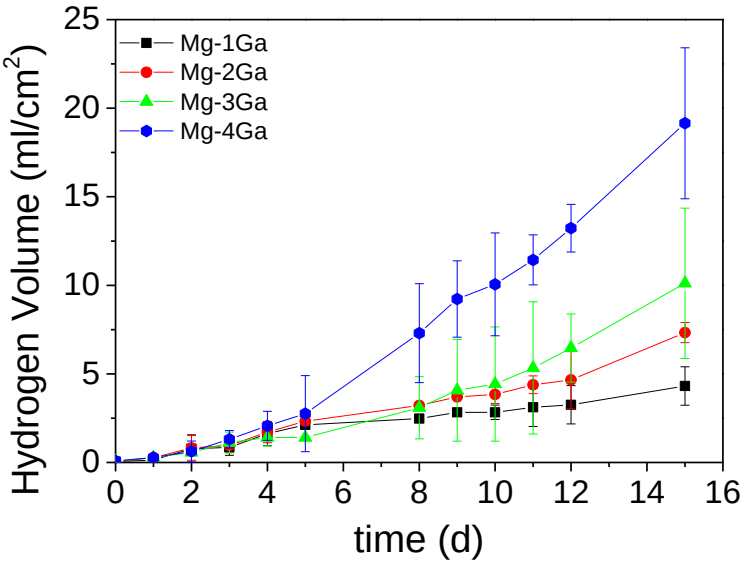

Figure 8. Hydrogen evolution measurements up to 15 days of immersion in NaCl 0.5 wt.% solution.

Table 6. Average corrosion rate calculated by mass loss and hydrogen evolution measurements after 15 days of immersion in NaCl 0.5 wt.% aerated solution

	Average corrosion rate (mg cm^{-2} d^{-1})	
Material	Mass loss	Hydrogen evolution
Mg-1Ga	0.23±0.05	0.22±0.04
Mg-2Ga	0.32±0.03	0.48±0.06
Mg-3Ga	0.88±0.3	0.82±0.4
Mg-4Ga	1.38± 0.37	1.72± 0.4

3.2.3 Electrochemical measurements: Potentiodynamic polarization and electrochemical impedance spectroscopy (EIS)

Electrochemical methods were used as an indicative of the repassivation characteristics of the alloys.

Figure 9 shows the polarization curves for the materials after 30 min of immersion in aerated and stirred neutral 0.5 wt.% NaCl solution. For short immersion time, the differences in corrosion rate (obtained by Tafel extrapolation method based on the cathodic branch) are relatively small as well as the variations between the three specimens of the same alloy (Table 7). One should understand that such an approach can be used only as indicative for comparison of similar systems. For this short immersion period, corrosion rates for all the studied materials are similar, which is in concordance with the hydrogen evolution data at the initial stages of the immersion.

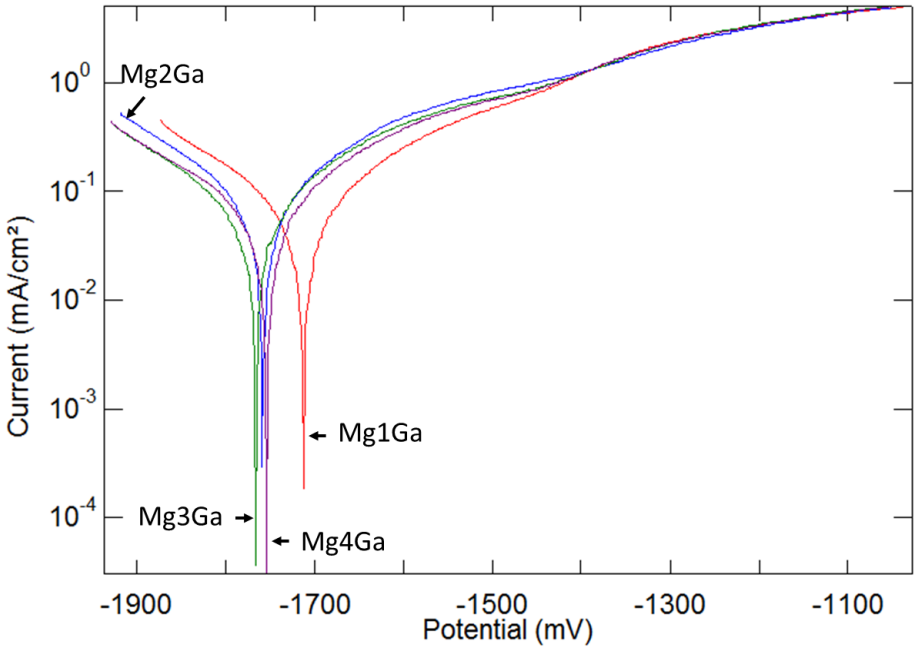

Figure 9. Polarization curves for the Mg-Ga alloys after 30 min of immersion in aerated and stirred neutral 0.5 wt.% NaCl solution.

Table 7. Results from OCP (30 min) and potentio-dynamic polarization measurements in aerated and stirred 0.5 wt. % NaCl solution

alloy	OCP (mV vs. Ag/AgCl)	Corrosion Potential (mV vs. Ag/AgCl)	Corrosion rate (mm/y)
Mg-1Ga	-1733 ± 8	-1723 ± 11	1.47 ± 0.06
Mg-2Ga	-1766 ± 3	-1754 ± 12	1.45 ± 0.37
Mg-3Ga	-1773 ± 1	-1764 ± 1	1.35 ± 0.11
Mg-4Ga	-1768 ± 9	-1753 ± 2	1.26 ± 0.09

To demonstrate the possibility of passivation again, EIS measurements were also performed directly after potentiodynamic polarization tests which were used to force the active dissolution once the film breakdown potential is exceeded. The results are displayed in Figure 10. It is

clearly visible that the specimens do recover and buildup a new protective film on the surface already 5 minutes after the polarization measurement was stopped. Only the alloy with 1 wt. % Ga required a recovery time of one hour to stop localized corrosion on the surface. Localized or pitting corrosion is normally related to the occurrence of an inductive loop in EIS measurements [28,29]. This loop is only visible for the Mg-1Ga alloy after 5 min. Between the first measurement at 5 min and the second one after 65 min the surface passivated again and the inductive loop disappeared. For the other three alloys no inductive loop was recorded at any time.

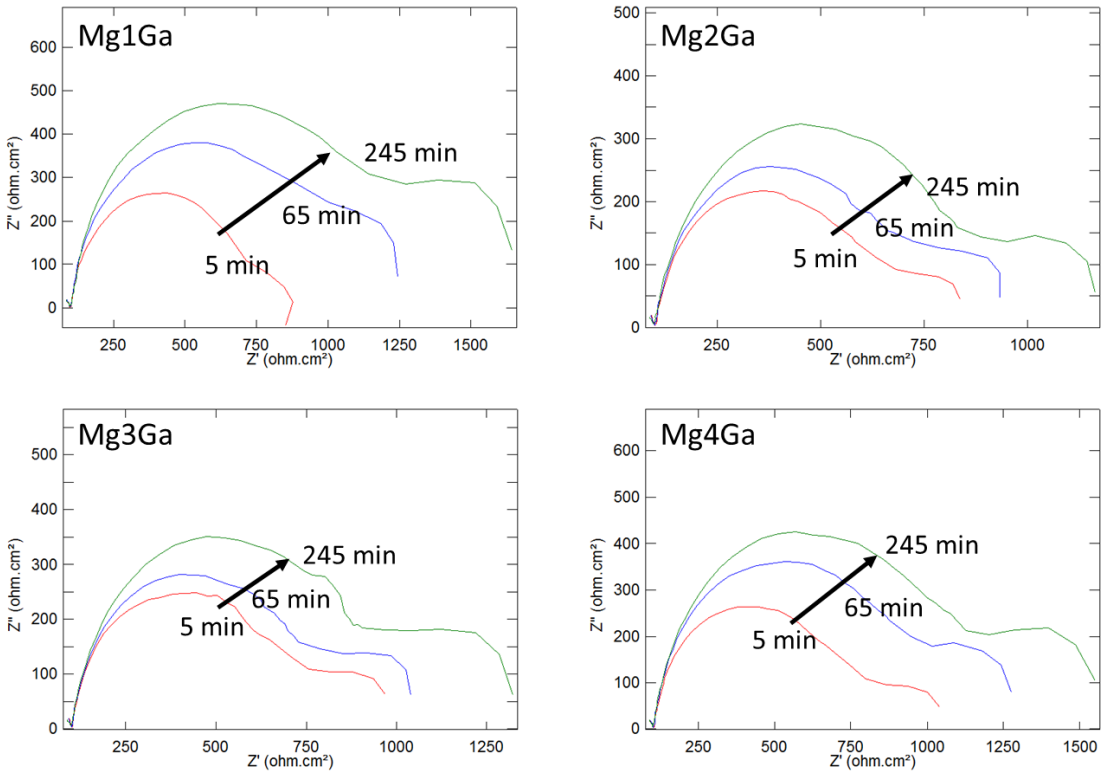

Figure 10. EIS measurements after potentiodynamic polarization in aerated 0.5% NaCl solution.

Figure 11 shows the Nyquist plots obtained for Mg-2Ga alloy (as a typical example) after immersion in 0.5 wt.% NaCl solution for various times up to 7 days. Curves recorded for the other alloys do look similar. They are normally characterized by a capacitive loop at high and

medium frequencies, indicating the formation of a partly stable passive film on the surface of the alloys, followed by a loop in the low-frequency region associated with the charge transfer resistance and double layer capacitance at the metal/solution interface.

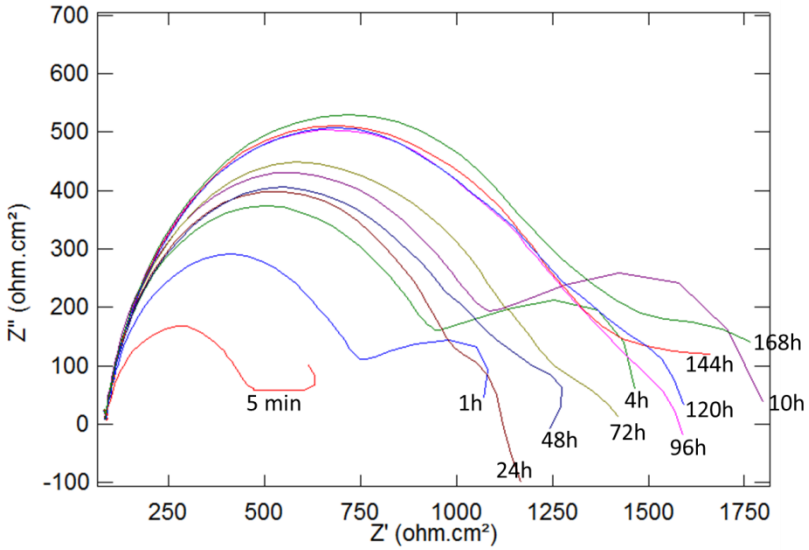

Figure 11. Typical impedance spectra for the alloys recorded during immersion in aerated 0.5% NaCl solution at RT. Example is showing the Mg-2Ga alloy with an early failure after 24 h immersion and slowly recovery of the protective film again.

The occurrence of an inductive loop in the spectra after 24 hours (Fig. 11) indicates failure of the film visible by active dissolution of substrate material combined with hydrogen formation from small localized areas. The film breakdown causes much lower impedance values (24h) than before the breakdown (10h) and it can take some time until the film fully recovers. All the alloys show such a failure of the corrosion products film during testing at different immersion times, but they are able to recover from such a localized attack. Some of the specimens especially at higher Ga contents do show sequences of failure and passivation events at different locations on the specimen. To demonstrate this behavior the low frequency impedance values measured at 0.01 Hz taken at the different immersion times of all specimen are summarized in Fig. 12. They can be considered as a simple indicator of the DC corrosion resistance of the

specimens at the time of measurement and show that the possible maximum film resistance as well as the tendency for film breakdown seems to increase with Ga concentration. The latter is visible in higher error values observed in the average film resistance with increasing amount of Ga (Fig. 12). The variations not only indicate that the times of film breakdown and recovery times do change from specimen to specimen but demonstrate also an increasing difference between active and passive states with increasing Ga content. As already indicated by the polarization measurements and the subsequent EIS measurements, the long-term EIS measurements without pre-damage also confirm that the specimen does not tend to strong localized corrosion and the main corrosion mechanism is general corrosion. The most uniform and predictable corrosion under the test conditions used for impedance measurements is obtained for the Mg-2Ga alloy.

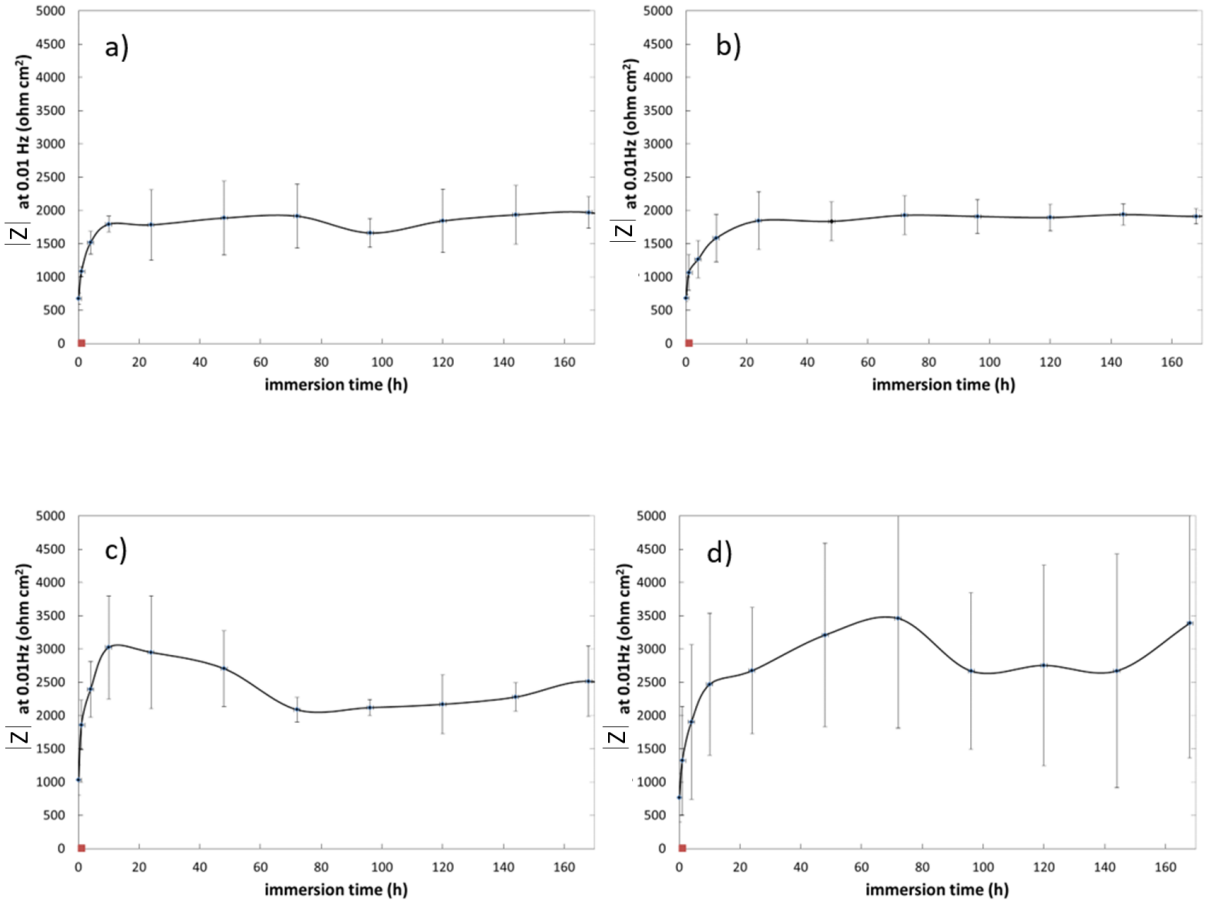

Figure 12. Development of low frequency impedance modulus values with immersion time of up to 168 hours in stirred aerated 0.5% NaCl solution for the different alloys a) Mg-1Ga, b) Mg-2Ga, c) Mg-3Ga and d) Mg-4Ga. The average values and the standard deviation (error bars) displayed are based on three measurements performed with three different specimens per alloy.

3.2.4 X-ray photoelectron spectroscopy (XPS)

All of the studied Mg-Ga alloy systems were investigated by XPS measurements. The as-received materials as well as the samples after exposure to EIS measurements (7 days of immersion in 0.5 wt.% NaCl at room temperature) have been characterized. From the survey spectra (Figure 13) the regions of elements for further investigations were defined. To get information on composition of any passive or corrosion product layer, a depth profiling by argon etching was additionally carried out for 4500 seconds. Related to a calibrated removal rate of 12 nm/min for Ta_2O_5 this is approximately a depth of 900 nm. After each 600 seconds survey spectra and regions of Mg 2p, Ga 2p, O 1s and C 1s have been recorded. Unfortunately, the instrumental power for the compensation of charges which have been caused by amorphous material and Ar ion bombardment during etching could not be increased to get a complete charge neutralization. As result, the region data for Mg 2p and O 1s show some undefined peak shapes that made an exact deconvolution impossible. However, the region for Mg 2p can be defined as total Mg amount consisting of Mg (49.9 eV binding energy) as well as MgO (50.8 eV) while the O 1s region includes various oxides (Mg, Ga) in the range of 528 to 533 eV.

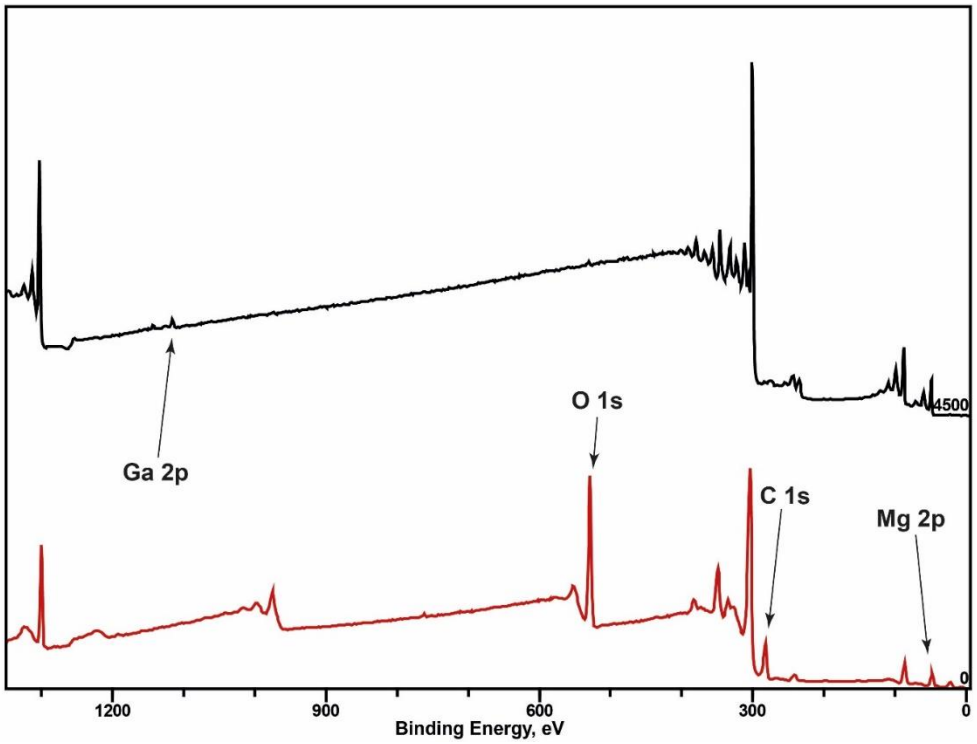

Figure 13. XPS survey spectra of Mg-1Ga as-received at 0 etching time (bottom) and after 4500 seconds (top).

Figure 14 shows the depth profiles for Mg-1Ga and Mg-4Ga exemplarily before and after EIS experiments. For all alloy compositions, an oxidation layer was detected. Additionally, carbon is present on the outermost surface which corresponds to adsorbed CO_2 from the environment. However, in case of the as received Mg-1Ga the oxidation layer has a thickness of about 480 nm (2400 sec of Ar etching). After that time the Mg concentration is above 95 at-% and the oxygen concentration is below 4 at-% which is in the range of the amount of oxygen in the bulk material. For higher amounts of Ga in the as received alloy the MgO layer is much more developed (Figure 14 c). After 4500 seconds (~ 900 nm) the 90 at-% line for Mg cannot be reached.

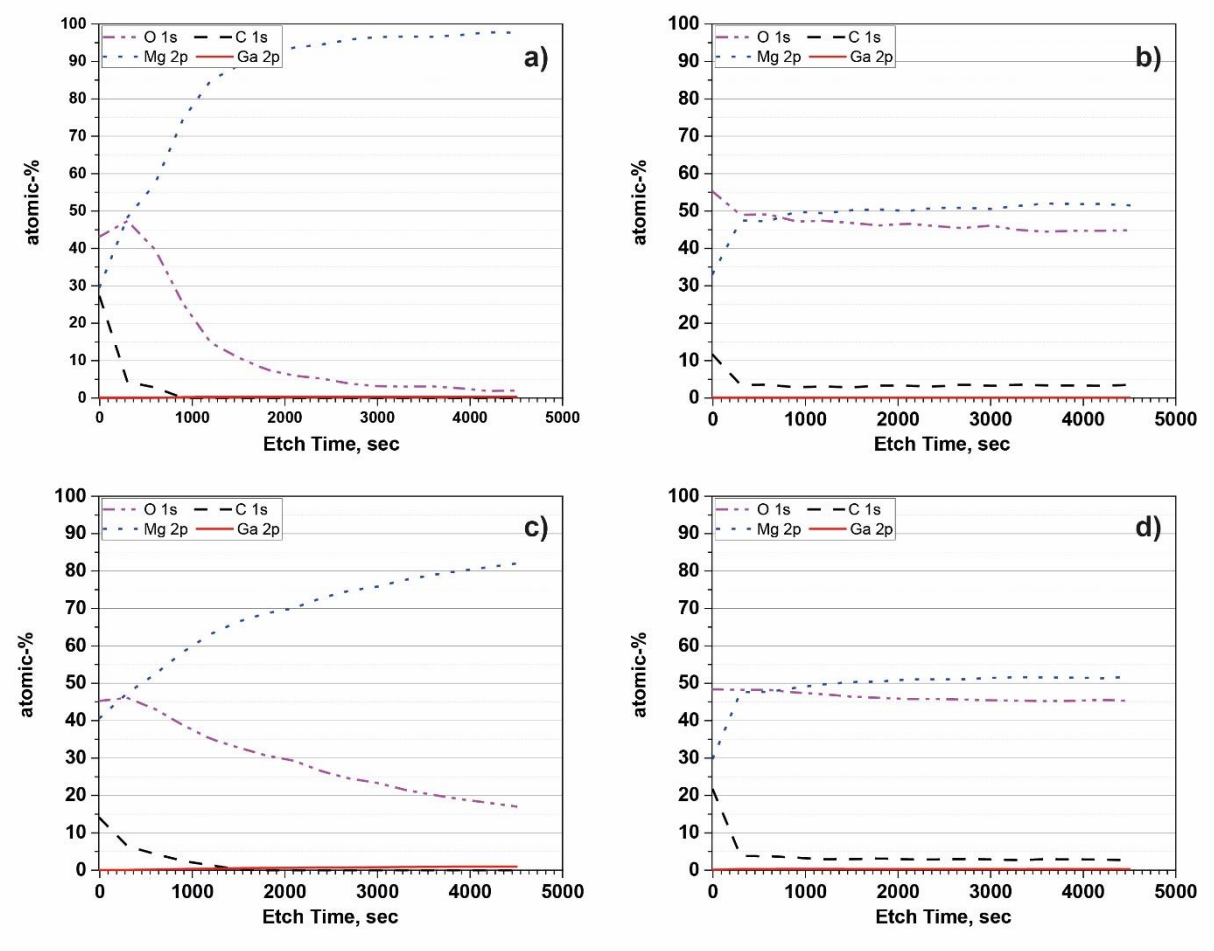

Figure 14. XPS depth profiles of (a) Mg-1Ga as-received (b) Mg-1Ga after exposure to electrolyte (EIS measurement) (c) Mg-4Ga as-received (d) Mg-4Ga after exposure to electrolyte (EIS measurement) (removal rate: 12 nm/min related to Ta_2O_5)

The evaluation of the region data presented in Figure 15a, c and Figure 16 a, c confirms this extension of the oxide layer. While for as-received Mg-1Ga the Mg 2p signal shifts after 1200 sec from the MgO state (51 eV) to the Mg state (50 eV) the O 1s signal (531 eV) shows the corresponding decrease in concentration and nearly disappears after 2400 sec of Ar ion etching. The O 1s signal for Mg4Ga is still detectable after 4500 seconds and shows by its shape that certain oxides still exist in very low concentration. Moreover, all Figures of the as-received materials show that Ga is almost not present in the outermost layer but its concentration increases after a period of 1200 to 2400 seconds (approx. 240 to 480 nm) to reach a final value.

After EIS measurements all materials (7 days of immersion in NaCl 0.5 wt. % at room temperature) show MgO for the complete depth profiling period of 4500 seconds (Figure 14 (b, d), 15 (e-h) and 16 (e-h)). The atomic concentration ratio for Mg to O is nearly 1:1 which confirms the existence of MgO. Traces of environmental contamination by CO_2 are removed directly after 600 seconds of argon etching. Therefore, these contaminations do not exist below 120 nm in depth and MgO dominates the layer. In opposite to the as-received material, Ga can be detected at the outermost surface layer. This confirms its participation in the corrosion processes during exposure to electrolyte from the very beginning. The concentration difference with its final concentration after about 500 nm is negligible and indicates a homogenous distribution in the corrosion layer.

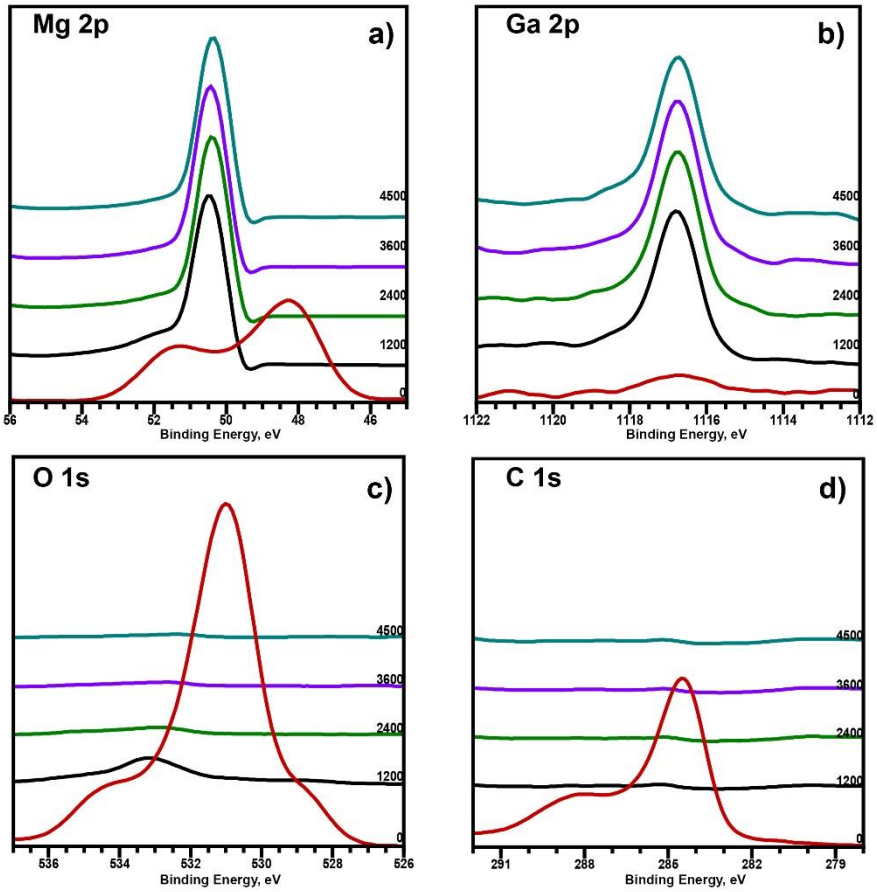

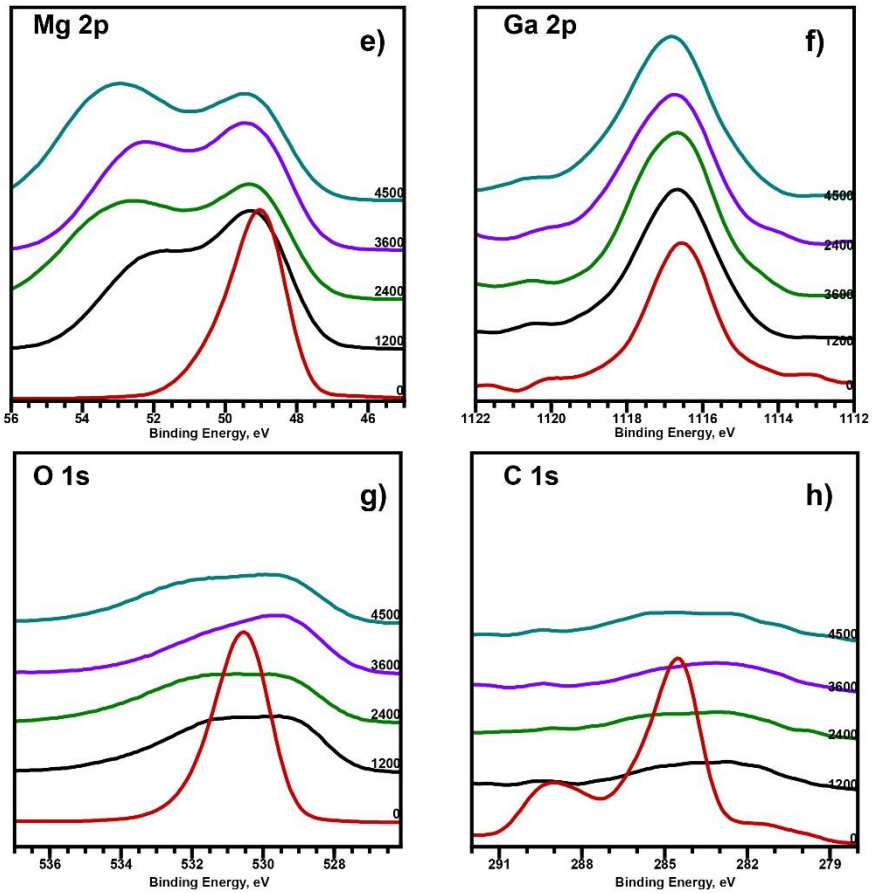

Figure 15. XPS regions for (a,b,c,d) Mg-1Ga as-received at 0 etching time and after 1200, 2400, 3600 and 4500 seconds and (e,f,g,h) Mg-1Ga after EIS measurements at 0 etching time and after 1200, 2400, 3600 and 4500 seconds.

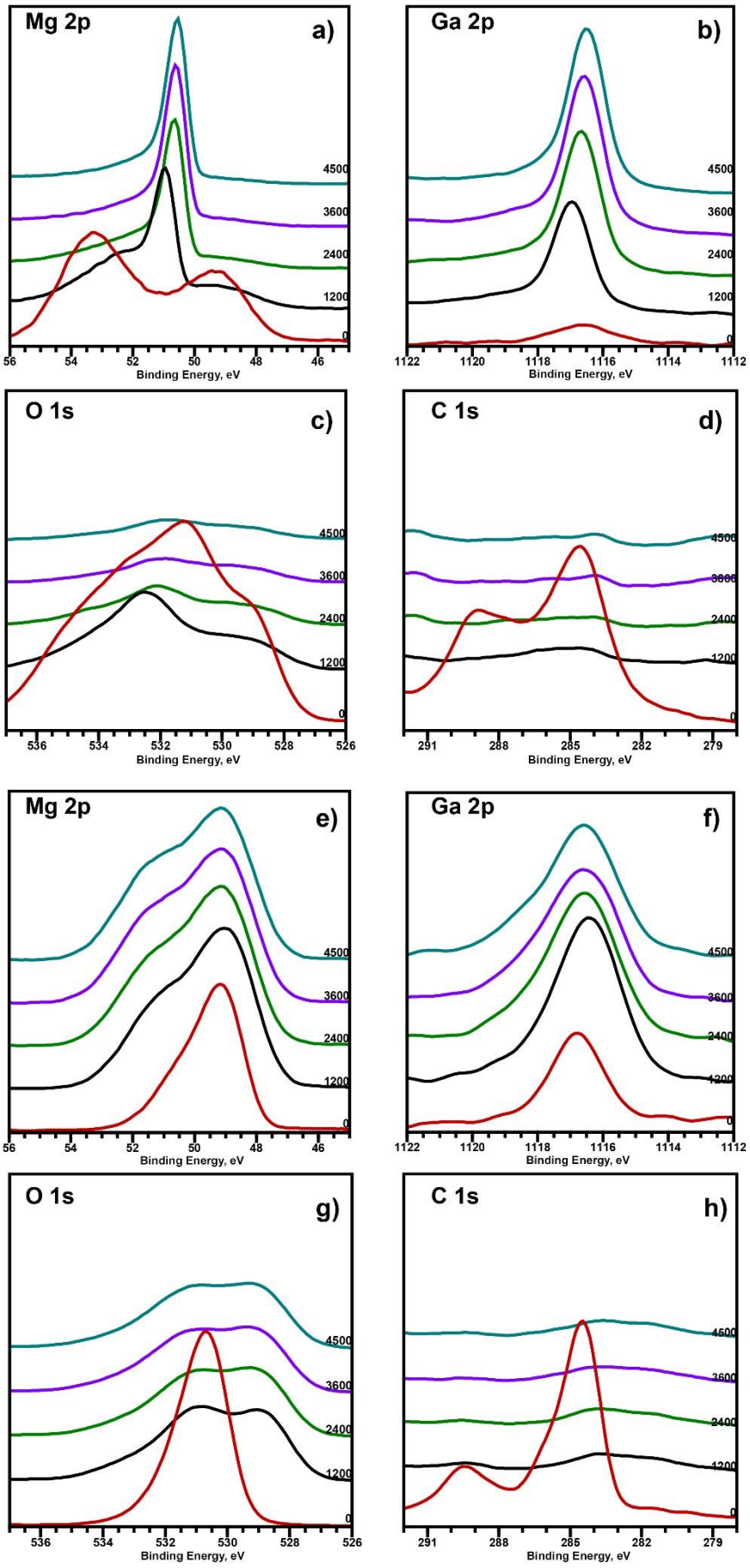
Mg 2p
a)
4500
3600
2400
1200
0
56
54
52
50
48
46
Binding Energy, eV
Ga 2p
b)
4500
3600
2400
1200
0
1122
1120
1118
1116
1114
1112
Binding Energy, eV
O 1s
c)
4500
3600
2400
1200
0
536
534
532
530
528
526
Binding Energy, eV
C 1s
d)
4500
3600
2400
1200
0
291
288
285
282
279
Binding Energy, eV
Mg 2p
e)
4500
3600
2400
1200
0
56
54
52
50
48
46
Binding Energy, eV
Ga 2p
f)
4500
3600
2400
1200
0
1122
1120
1118
1116
1114
1112
Binding Energy, eV
O 1s
g)
4500
3600
2400
1200
0
536
534
532
530
528
526
Binding Energy, eV
C 1s
h)
4500
3600
2400
1200
0
291
288
285
282
279
Binding Energy, eV

Figure 16. XPS regions for (a,b,c,d) Mg-4Ga as-received at 0 etching time and after 1200, 2400, 3600 and 4500 seconds and (e,f,g,h) Mg-4Ga after EIS measurements at 0 etching time and after 1200, 2400, 3600 and 4500 seconds.

4. Discussion

The increase of the amount of Ga from 1 to 4 wt.% has the following effects on the microstructure of the Mg-Ga alloys: (i) a refinement of the grain size, (ii) an increase of the second phase (Mg_5Ga_2) fraction, (iii) slightly higher hardness values (not significant). The eutectic phase was identified as Mg_5Ga_2, which is normally found in Mg-Ga binary [23] and Mg-Hg-Ga ternary [20] alloys. In addition, inclusions containing impurities (Fe, Co) were observed. In this study and for the first time, the electrochemical characterization of these different intermetallic particles on Mg-Ga alloys is reported, confirming the capabilities of SKPFM method. It is worth to mention that Mg_5Ga_2 phase having a VPD vs matrix around +75 mV did not cause a strong localized corrosion during short term immersion in NaCl solution. However, significantly higher susceptibility to localized corrosion is shown for the particles containing heavy metal with a VPD high enough to form an active galvanic couple. This key role of impurities on the corrosion of Mg-Ga alloys is in accordance with previous research on other Mg-based materials [30,31].

In the case of widely studied Mg-Al alloys, an extensive range of VPD values for the second phase β-$Mg_{17}Al_{12}$ has been reported with controversial results in the cathodic character of this phase (with VPD from 50mV to 200mV) [32-35]. For Ga-containing Mg alloys, a few studies point out that the corrosion properties are strongly influenced by the morphology and distribution of second phases ($Mg_{21}Ga_5Hg_3$ and Mg_5Ga_2) acting as cathodes [19,20]. However, these studies are limited in the following terms: (i) they are only focused on the Mg-Hg-Ga

system, (ii) the values of VPD are not reported (ii) the effect of impurities is not considered. In fact, the present study reveals that only the inclusions containing impurities can act, at initial stage, as an active cathode for microgalvanic corrosion.

Findings reveal that the average corrosion rate of the Mg-(1-4) wt.% Ga alloys in 0.5 wt.% NaCl aqueous solution during 15 days exposure increases with the addition of Ga as measured by weight loss and hydrogen evolution. This trend is in accordance with the results obtained by Y. Feng et al. in the ternary systems Mg-5 at. % Hg- (1, 5, 22) at %. Ga, with an increase of the corrosion rate for Ga addition higher than 1 at.% after immersion in 3.5 wt.% NaCl [36]. J. Kubasek et al. [23] also found the same tendency for Mg-(1, 4, 7) wt.% Ga alloys immersed in 0.9 wt.% NaCl, with faster corrosion rates for Ga addition higher than 1 wt.%, due to an increase of microgalvanic corrosion with the second phase Mg_5Ga_2. However, this last statement was not confirmed by any localized corrosion measurement. The results obtained in this work suggest that the second phase Mg_5Ga_2 does not play an important role as starting point for microgalvanic activities, when it does not contain Fe impurities. However, an increase in the volume of second phase also increases the cathodic/anodic area, causing a faster dissolution of the α-Mg matrix at prolonged immersion times.

The mechanism of relatively uniform corrosion is supported by the electrochemical results: (i) specimens are able to recover and form a new protective layer after forced breakdown due to polarization (ii) EIS measurements for specimens without pre-polarization show failure of the passive film during the experiments, but also a recovery with the consequent formation of a new protective layer of corrosion products. The highest values of the impedance modulus during one week of immersion are obtained for the alloys containing 3 and 4 wt.% Ga and this fact is related with the formation of a thicker oxide layer as was confirmed by XPS analysis. Even before the corrosion test, just in contact with air, the Mg-4Ga alloy forms a thicker oxide layer. This faster formation of corrosion products with increasing amount of Ga, may be related with the change in the cathodic/anodic area, leading to a faster dissolution of the α-Mg matrix.

It is important to highlight that the variation of the film resistance and the tendency for the film breakdown increase with Ga concentration, indicating the non-protective character of this film if it gets too thick. In fact for longer times of immersion (up to 15 days) significant differences of the corrosion rates were found measured by weight loss and hydrogen evolution.

Based on the present results, the effect of Ga on the corrosion resistance of studied alloys in aqueous solutions is mainly related to these factors: (i) microgalvanic corrosion between α-Mg and second phases containing impurities: the presence of impurities with high VPD act as a starting point of electrochemical activities but with the time of immersion the oxide film covers the particles and the corrosion mechanism is driven by uniform corrosion (ii) Mg_5Ga_2-phase morphology and distribution: although the VPD between Mg_5Ga_2 and α-Mg matrix is not significant, increasing the amount of the second phase leads to an increase of the cathode to anode area ratio which is detrimental for the corrosion behavior but localized corrosion susceptibility is not increased (iii) the stability of the oxide layer: alloys containing higher amount of Ga develop faster a thicker corrosion corrosion products layer with more tendency to break down.

This study points out the potential of systems based on Mg-Ga as degradable biomaterials with relatively uniform form of corrosion attack avoiding a strong localized corrosion which normally compromises the mechanical stability of the implant. However, detailed studies of biocompatibility and the effect of organic additives on the corrosion performance (amino acids, proteins, vitamins, and antibiotics) should be carried out.

5. Conclusions

Mg-(1,2,3,4) wt.% Ga alloys present two types of intermetallics: (i) the second phase Mg_5Ga_2, which volume increases with the amount of Ga in the alloy, and (ii) inclusions containing

impurities. Mg_5Ga_2 phase does not show significant VPD compared to the α-Mg matrix. However, inclusions containing impurities reveal high VPD enough to form an active galvanic couple at the initial stage of corrosion.

Hydrogen evolution measurements display that at early stages of immersion, the studied alloys show similar corrosion behavior, without a clear effect of gallium concentration. For longer immersion times, concentrations of Ga higher than 2 wt.% lead to faster corrosion rates, confirmed by weight loss and hydrogen evolution measurements.

Electrochemical results revealed that alloys containing higher amount of Ga develop faster a corrosion products layer with more tendency to break down at later stages.

The corrosion behavior of the studied Mg-Ga alloys is associated with three main factors:

(i) Microgalvanic corrosion between α-Mg and second phases containing impurities but the localized electrochemical decrease with the immersion time.

(ii) Higher volume of Mg_5Ga_2, increases the cathode to anode area ratio which is detrimental for the corrosion behavior.

(iii) The formation and stability of the oxide layer

Acknowledgments

MM is grateful to the MICINN (Spain) for financial support via Juan de la Cierva Programme (IJCI-2014-19117), Proyecto Retos Jovenes Investigadores (MAT2015-73355-JIN) and to the Alexander von Humboldt Foundation (Germany). This work has been financial supported by Comunidad de Madrid (MULTIMAT-CHALLENGE, Ref: P2013/MIT-2862) and MICINN (Spain, Project MAT2015-66334-C3-3-R). The technical support from Mr. U. Burmester and Mr. V. Heitmann is gratefully acknowledged.

Figures

Figure 1. Optical micrographs of (a) Mg-1Ga, (b) Mg-2Ga, (c) Mg-3Ga and (d) Mg-4Ga alloys.

Figure 2. TEM analysis: (a) Second phase (b) electron diffraction pattern of the second phase (c,d) polygonal-shape particles containing impurities.

Figure 3. Scanning electron micrograph of the Mg-4Ga (a) lower magnification (b) a detail of the second phase Mg_5Ga_2.

Figure 4. Mg-4Ga sample: (a) surface topography (b) SKPFM image and (c) VPD profile across the grain.

Figure 5. Mg-4Ga sample: (a) surface topography (b) SKPFM image and (c) and a VPD profile across the intermetallic and impurity; (d) EDS analysis of an impurity and intermetallic.

Figure 6. Mg-4Ga sample: (a,b,c) surface topography before and after immersion (20 and 40 min) in diluted NaCl solution, (d,e,f) SKPFM before and after immersion (20 and 40 min) in diluted NaCl solution (g) VPD profiles across the Mg_5Ga_2 intermetallic.

Figure 7. Mg-4Ga sample: (a,b,c) surface topography before and after immersion (20 and 40 min) in diluted NaCl solution, (d,e,f) SKPFM before and after immersion (20 and 40 min) in diluted NaCl solution (g) VPD profiles across the Mg_5Ga_2 intermetallic and impurity.

Figure 8. Hydrogen evolution measurements up to 15 days of immersion in NaCl 0.5 wt.% solution.

Figure 9. Polarization curves for the Mg-Ga alloys after 30 min of immersion in aerated and stirred neutral 0.5 wt.% NaCl solution.

Figure 10. EIS measurements after potentiodynamic polarization in aerated 0.5% NaCl solution.

Figure 11. Typical impedance spectra for the alloys recorded during immersion in aerated 0.5% NaCl solution at RT. Example is showing the Mg-2Ga alloy with an early failure after 24 hour immersion and slowly recovery of the protective film again.

Figure 12. Development of low frequency impedance values with immersion time of up to 168 hours in stirred aerated 0.5% NaCl solution for the different alloys a) Mg-1Ga, b) Mg-2Ga, c) Mg-3Ga and d) Mg-4Ga. The average values and the standard deviation (error bars) displayed are based on three measurements performed with three different specimens per alloy.

Figure 13.XPS survey spectra of Mg-1Ga as-received at 0 etching time (bottom) and after 4500 seconds (top).

Figure 14. XPS depth profiles of (a) Mg-1Ga as-received (b) Mg-1Ga after exposure to electrolyte (EIS measurement) (c) Mg-4Ga as-received (d) Mg-4Ga after exposure to electrolyte (EIS measurement) (removal rate: 12 nm/min related to Ta_2O_5)

Figure 15. XPS regions for (a,b,c,d) Mg-1Ga as-received at 0 etching time and after 1200, 2400, 3600 and 4500 seconds and (e,f,g,h) Mg-1Ga after EIS measurements at 0 etching time and after 1200, 2400, 3600 and 4500 seconds.

Figure 16. XPS regions for (a,b,c,d) Mg-4Ga as-received at 0 etching time and after 1200, 2400, 3600 and 4500 seconds and (e,f,g,h) Mg-4Ga after EIS measurements at 0 etching time and after 1200, 2400, 3600 and 4500 seconds.

Tables

Table 1. Composition analysis in wt. % for the studied materials using spark spectrum emission analysis (for the heavy metal contaminations) and EDS large area analysis (for Ga).

Table 2. Composition determined by point analysis EDS (at.%) for Figure 2 (c,d).

Table 3. Hardness measurements (HV).

Table 4. Composition determined by point analysis EDS (at.%) for Figure 3 b.

Table 5. VPD levels on magnesium alloys, intermetallics and impurities; at least 15 different intermetallics or impurities were analysed in order to calculate ΔVPD levels.

Table 6. Corrosion rate calculated by mass loss and hydrogen evolution measurements after 15 days of immersion in NaCl 0.5 wt.% aerated solution

Table 7. Results from OCP (30 min) and potentio-dynamic polarization measurements in aerated and stirred 0.5% NaCl solution

References

1. H. Westengen, Magnesium Alloys: Properties and Applications, Encyclopedia of Materials: Science and Technology, (2001) 4746-4753.
2. E. Ghali, Magnesium and magnesium alloys .W. Revie (Ed.), Uhlig's Corrosion Handbook, John Wiley & Sons, New York, 2000.
3. A. Pardo, M.C. Merino, A.E. Coy, R. Arrabal, F. Viejo, E. Matykina, Corrosion behaviour of magnesium/aluminium alloys in 3.5 wt.% NaCl, Corros. Sci., 50 (2008) 823-834.
4. M. Jönsson, D. Persson, The influence of the microstructure on the atmospheric corrosion behavior of magnesium alloys AZ91D and AM50, Corros. Sci., 52 (2010) 1077-1085.
5. G. Baril, C. Blanc, M. Keddam, N. Pebere, Local electrochemical impedance spectroscopy applied to the corrosion behaviour of an AZ91 magnesium alloy, J. Electrochem. Soc. 150 (2003) B488-B493.
6. H. Pan, Y. Ren, H. Fu, H. Zhao, L. Wang, X. Meng, G. Qin, Recent developments in rare-earth free wrought magnesium alloys having high strength: A review, J. Alloy. Comp. 663 (2016) 321-331
7. T. Takenaka, T. Ono, Y. Narazaki, Y. Naka, M. Kawamaki, Improvement of corrosion resistance of magnesium metal by rare earth elements, Electrochim. Acta, 53 (2007) 117-121.
8. R. P. Beck. The EMF properties of magnesium and thermal analysis of the Mg-Hg system, Recl. Trav. Chim. Pays-Bas, 41 (1922) 353-399.
9. A.A. Nayeb-Hashemi, J.B. Clark, Bull, Alloy Phase Diagram, 6 (1985) 434-439.
10. Y. Feng, R. Wang, H. Liu, Z. Jin, Thermodynamic reassessment of the magnesium–gallium system, J. Alloys Compd., 486 (2009) 581-585.

11. J. C. McDonald, M. Mich, Magnesium base alloy, patent N° 371375.
12. H. Liu, G. Qi, Y. Ma, H. Hao, F. Jia, S. Ji, H. Zhang, X. Zhang, Microstructure and mechanical property of Mg-2.0Ga alloys, Mat. Sci. Eng. A, 526 (2009) 7-10. 2656.
13. Y. Geng, R. Wang, C. Peng, Influence of Ga and In on microstrcuture and electrochemical properties of Mg anodes, T. Nonferr. Metal Soc., 23 (2013) 2650-2656.
14. J. Zhao, K. Yu, Y. Hu, S. Li, X. Tan, F. Chen, Z. Yu, Discharge behavior of Mg–4 wt%Ga–2 wt%Hg alloy as anode for seawater activated battery, Electrochim. Acta, 56 (2011) 8224-8231.
15. D. Wu, L. Ouyang, C. Wu, H.Wang, J. Liu, L. Sun, M. Zhu, Phase transition and hydrogen storage properties of Mg–Ga alloy, J. Alloys Compd., 642 (2015) 180-184.
16. D. O. Flamini,S. B. Saidman, J. B. Bessone, Aluminium activation produced by gallium, Corros. Sci. 48 (2006) 1413-1425.
17. Y. Feng, R. C. Wang, C. Q. Peng, Influence of alloying elements Ga and Hg on the electrochemical corrosion behaviour of Mg solid solution, Corrosion, 67 (2011) 055003-1-055003-6.
18. Y. Feng, R. Wang, K. Yu, C. Peng, J. Zhang, C. Zhang, Activation of Mg–Hg anodes by Ga in NaCl solution, J. Alloys Compd., 473 (2009) 215-219.
19. Y. Feng, R. Wang, K. Yu, C. Peng, N. Wang, Influence of $Mg_{21}Ga_5Hg_3$ compound on electrochemical properties of Mg-5%Hg-5%Ga alloy,T. Nonferr. Metal Soc., 19 (2009) 154-159.
20. Y. Feng, R. Wang, C. Peng, H. Tang, H. Liu, Influence of Mg_5Ga_2 compound on microstructures and electrochemical properties of Mg-5%Hg-22%Ga alloy, Prog. Nat. Sci., 21 (2011) 73-79.
21. Y. Xin, T. Hu, P.K. Chu, Influence of test solutions on in vitro studies of biomedical magnesium alloys, J. Electrochem. Soc., 157 (2010) C238-C243.

22. S. Virtanen, Biodegradable Mg and Mg alloys: Corrosion and biocompatibility, Mat. Sci. Eng. B, 176 (2011) 1600-1608.
23. J. Kubásek, D. Vojtech, J. Lipov, T. Ruml, Structure, mechanical properties, corrosion behavior and cytotoxicity of biodegradable Mg–X (X = Sn, Ga, In) alloys. Mat. Sci. Eng. B, 33 (2013) 2421-2432.
24. P. Melnikov, A.R. Teixeira, A. Malzac, M.D. Coelho, Gallium-containing hydroxyapatite for potential use in orthopedics, Mater. Chem. Phys., 117 (2009),86-90.
25. L. R. Bernstein, Mechanisms of therapeutic activity for gallium, Pharmacol. Rev., 50 (1998) 65-682.
26. G. Song, A. Atrens, D. St. John, An hydrogen evolution method for estimation of the corrosion rate of magnesium alloys, Magnesium Technol., (2001) 254-262.
27. A.E. Coy, F. Viejo, P. Skeldon, G.E. Thompson, Susceptibility of rare-earth-magnesium alloys to micro-galvanic corrosion, Corros. Sci., 52 (2010) 3896-3906.
28. S. Jin, S. Amira, E. Ghali, Electrochemical impedance spectroscopy evaluation of the corrosion behavior of die cast and thixocast AXJ530 magnesium alloy in chloride solution, Adv. Eng. Mater. 9 (2007) 75-83
29. M. Bobby Kannan, W. Dietzel, R. Zeng, R. Zettler, J.F. dos Santos, A study on the SCC susceptibility of friction stir welded AZ31 Mg sheet, Mater. Sci. Eng. A, 460-461 (2007) 243-250
30. G. Ballerini, U. Bardi, R. Bignucolo, G. Ceraolo, About some corrosion mechanisms of AZ91D Mg alloys, Corr. Sci., 47 (2005) 2173-2184.
31. O. Lunder, K. Nisancioglu, R.S. Hansen, Corrosion of die cast magnesium aluminium alloy, paper 930755 SAE, Congress and Exposition, Detroit, MI (1993)

32. S. Mathieu, C. Rapin, J. Steinmet, P. Steinmetz, A corrosion study of the main constituent phases of AZ91 magnesiumm alloys, Corros. Sci., 45 (2003) 2741-2755.
33. M. Jonsson, D. Thierry, N. LeBozec, The influence of microstructure on the corrosion behaviour of AZ91D studied by scanning kelvin probe force microscopy and scanning kelvin probe, Corros. Sci., 48 (2006) 1193-1208.
34. F. Andreatta, I. Apachiete, A. A. Kodentsov, J. Dzwonczyk, J. Duszczyk, Volta potential of second phase particles in extruded AZ80 magnesium alloy, Electrochim. Acta, 51 (2006) 351-357.
35. R. Arrabal, B. Mingo, A. pardo, E. Matykina, M. Mohedano, M.C. Merino, A. Rivas, A. Maroto, Role of alloyed Nd in the microstructure and atmospheric corrosion of as cast magnesium alloy AZ91, Corros. Sci., 97 (2015) 38-48.
36. Y. Feng, R. Wang, K. Yu, C. peng, W. Li, Influence of Ga content on electrochemical behavior of Mg-5at Hg anode materials, Mater. Trans., 49 (2008) 1077-1080.